Identification of black carbon in the brain using Raman microscopy.

Anthony G. Norman

A thesis

submitted in partial fulfillment of the

requirements for the degree of

Master of Public Health

University of Washington

2021

Committee:

Coralynn Sack

Dan Fu

Joel Kaufman

Program Authorized to Offer Degree:

Environmental and Occupational Health Sciences

University of Washington

ABSTRACT

Identification of black carbon in the brain using Raman microscopy.

Anthony G. Norman

Chair of the Supervisory Committee:

Coralynn Sack

Departments of Environmental and Occupational Health Sciences, Medicine

Introduction: Air pollution is a significant contributor to adverse health outcomes in humans around the world. Particulate matter has been linked to numerous cardiovascular, pulmonary and neurological diseases and associated with increased systemic inflammation and direct cellular toxicity. Earlier studies have suggested three potential routes of entry for particulate matter into the central nervous system: systemic circulation and active transport into cells; leaky capillaries compromising the blood-brain barrier allowing for infiltration of the parenchyma or translocation along the olfactory system. Newer imaging technologies have been developed to allow for direct, non-destructive molecular identification of compounds through excitation of the molecular chemical bond vibrational energies, with minimal preparation. The use of Raman microscopy of multiple varieties, in particular, is quickly expanding throughout the biological sciences. We sought to identify the carbon core material of ultrafine particulate matter in the CNS of mouse and human subjects with known or estimated exposures to diesel exhaust or air pollution,

respectively, using Raman microscopic techniques. **Methods:** Three groups of tissues were examined. First, mouse alveolar macrophages were exposed to increasing concentrations of diesel exhaust particles (DEP) and imaged with stimulated Raman scattering (SRS) microscopy. Second, a small group of naïve and experimental mice perinatally exposed to diesel exhaust (DE) were sacrificed and their brain tissues directly imaged with SRS along the olfactory bulb, corpus callosum and frontal lobes to identify areas of potential DEP deposition. Third, human brain biopsies from subjects participating in the Adult Changes in Thought (ACT) study were obtained and also imaged with SRS along the olfactory, cerebellar and frontal lobe tissues for signs of black carbon particulate matter to be quantified and compared to estimated individual air pollution exposures. **Results:** The macrophage study readily identified the DEP and image analysis suggested a dose-dependent response to the uptake of DEP by the macrophages in a positive, linear fashion, though also with a wide variation in material uptake and extracellular particulate matter seen at most inoculating concentrations. Imaging of the mouse CNS tissues was successful at identifying several large structural features of the parenchyma as well as cellular elements such as red blood cells remaining in the larger blood vessels, as well as likely glial and neuronal cells. Particulate matter was not positively identified between the naïve and DE exposed subjects, however. Imaging of the human brain tissues was complicated by inadequate tissue thickness and the use of a paraffin based embedding media, which created a complex background spectral and fluorescence response. Identification of cellular and parenchymal structures was difficult and no particulate matter was found or distinguished from the background signal intensity. **Discussion:** SRS is a useful technique to identify the unique molecular response of DEP from surrounding biological material. The dose response relationship established with *in vitro* exposure of DEP to alveolar macrophages provides a basis for future,

more established studies to build upon. There are numerous potential technical and biological reasons for not being able to identify particles in the mouse CNS tissues, including inadequate resolution of the microscope system, inappropriate specimen preparation or sampling error versus the particulate matter not reaching the deeper tissues of the brain or otherwise being cleared over time. There are numerous similar reasons for being unable to identify the particles in the human biopsy samples, the most likely of which is the inadequate specimen preparation for the SRS microscope. Further study is required to fully determine the potential efficacy of SRS in the process of identifying particulate matter within the CNS and potential correlation to inflammatory induction or similar responses.

TABLE OF CONTENTS

LIST OF FIGURES

LIST OF TABLES

ACKNOWLEDGEMENTS

We would first like to thank all of the investigators, assistants, and administrators of the Adult Changes in thought study at Kaiser for continuing their study and allowing us access to the human tissue samples. Their continued hard work and willingness to share their data was incredible.

Next, Lianne Sheppard, Rachel Shaffer and the rest of their research group for the spatio-temporal exposure data and assistance in selecting subjects for our study.

Collin White and the Kavanaugh lab for assistance by creating the diesel soot exposed alveolar macrophage control series and suggestions on additional approaches to consider.

Elena Thomas for her efforts and trouble shooting the initial microscope imaging protocols and Helen Men for continuing those efforts and collecting all of the imaging data. We would also like to acknowledge the rest of the Fu research group for allowing our project to tuck into available time on the microscope during a time of significant challenges in scheduling.

I would like to acknowledge all my mentors in the Occupational and Environmental Medicine residency for sharing their clinical wisdom, research ideas and overall support throughout my training.

Finally, all my friends and family who have been supportive throughout the years of my medical school, residency and fellowship trainings. Your love and support have kept me moving forward even when there did not appear to be a way.

DEDICATION

To my wife, Jennifer Norman, who's encouragement and support made this all possible. Without you, I would be leading a much duller life and not have found myself in this training program.

Chapter 1. INTRODUCTION

Air pollution (AP) is a leading cause of global morbidity and mortality, contributing to adverse effects in the nervous, respiratory, and circulatory systems throughout all stages of life.(1-10) The global burden of disease estimates ranked Ambient $PM_{2.5}$ as the 5th most mortality risk factor in 2015, contributing to 4.2 million deaths, representing a 20% increase from 1990.(1) AP consists of a complex and dynamic mixture of gases and particles arising from the combustion of most all fuels.(9, 11) Many of the individual components affect human health through biochemical and genetic processes at all stages of life, from fetal development through old age.(2, 6, 12-18) Extensive research continues to be performed to better characterize and understand the precise nature of these effects in an effort towards developing better treatments of these diseases and preventative techniques to reduce the overall disease burden on society.

Exposure to particulate matter, specifically particles with aerodynamic diameter less than 2.5μm ($PM_{2.5}$), has been associated with developing Alzheimer's disease (AD) and Parkinson's disease (PD) due to neurotoxicity associated with neuroinflammation and increased oxidative stress from the presence of the particles as well as the adsorbed components of AP.(18-21) Summaries of exposure routes and mechanisms of toxicity are presented in Figures 1.1 and 1.2.(22, 23)

Of greatest interest are the ultrafine particles (< 0.1 μm diameter) as they may be able to translocate across the respiratory epithelium, and other barriers, to be distributed throughout the body via the circulatory system. Recently, several experimental studies suggest ultrafine particles may enter the brain through translocation via the olfactory bulb, in addition to crossing the blood-brain barrier via the circulatory system.(20, 24-30) The exact mechanism of such transport along

the olfactory tract remains to be discovered as well as the regions of the brain most likely to receive such particles once they cross into the central nervous system.

Air pollution has been an area of intense study by numerous stakeholders, including environmental scientists, regulatory agencies, and public health officials. As increased concern developed over the environmental and health impacts AP contributed to, regulatory agencies began to aggressively collect data on local atmospheric conditions and concentrations of the primary constituents of AP, mainly particulate matter (PM), oxides of nitrogen (NO_x) and Sulfur (SO_x), Carbon Monoxide (CO), Ozone (O_3) and trace metals. Starting in 1978 in the Puget Sound region, a wide range of regulatory and scientific instrumentation were placed seeking to better understand the patterns of AP as well as establishing and enforcing new air quality standards. As technologies increased and improved over the years, more, and less expensive, monitors were developed, allowing for better understanding of exposures the local populations were experiencing at a neighborhood level.(31-33) This data has since been utilized to develop models of individual exposures to AP based upon their addresses over several time periods. Efforts are now turning to methods of quantifying personal exposures through the use of a biomarker(s) so as to determine a given exposure's risks and characterize a broader dose response curve.(34, 35)

Over the last 10 years, newer methods of imaging have been developed allowing for the visualization of cellular molecular transport and metabolic processes using live cells, in addition to three-dimensional imaging of larger organelles and molecular constructs. These techniques utilize pulsed lasers and a series of diffraction or transmission offsets to induce refraction or fluorescence patterns dependent upon the molecular bonds and atomic structures present in the specimens with which they interact. RAMAN microscopy is one of these techniques becoming more rapidly utilized to investigate structure and metabolic processes within biological tissues.(36)

A subset of RAMAN imaging, stimulated Raman scattering (SRS), has become the forerunner for such investigations due to considerably faster imaging speed and increasingly finer resolutions.(37-46) These imaging techniques provide the ability to acquire large amounts of data over relatively short acquisition times when compared to traditional RAMAN microscopy. SRS microscopy uses coherent near-infrared laser beam(s) to detect characteristic molecular vibrations from the sample constituents allowing for the localization of specific molecules within the field of view, quantification of molecules of interest and development of a three-dimensional image to better understand the molecular interactions.

Understanding of the mobility of black carbon and other ultrafine particles throughout the body is potentially a valuable research tool if their accumulation in tissues of interest correlates to measured and/or estimated exposures. Earlier studies have detected inflammatory markers in CSF which correlated loosely with estimated AP exposures, but such markers are very non-specific and of limited use in a clinical setting. Furthermore, little is known about whether tissues are specifically impacted through particulate uptake or changes in the local environments as part of the immune response to the presence of such particles.

This pilot project was performed to investigate the questions of whether ultrafine particulate matter enters the central nervous system in a direct fashion and, if so, where it may aggregate. Additionally, we were seeking to establish whether a correlation existed between the amounts of particulate matter identified in CNS tissues and the estimated individual exposures. This investigation utilized a subset of subjects from a large prospective cohort study of aging and brain health.(47) Earlier projects have established models to estimate chronic exposure to particulate matter on an individual level(48) and we are looking to build upon those efforts through non-

destructive microscopic analysis of the molecular elements present within specific regions of the brain.

Investigators have recently developed predictive spatio-temporal models to estimate the individual long-term (40 years) average exposures of ambient pollution from residential addresses.(48-50) These models have been validated and correlate well with measured air pollution throughout the Puget Sound region from 1978 to the present, yielding a cross-validated R^2 (R^2_{cv}) of 0.87 and root mean square error (RMSE) of 1.29 $\mu g/m^3$ at the regulatory monitoring sites and $R^2_{cv} = 0.78$, RMSE = 0.89 $\mu g/m^3$ at the low cost measurement sites. This model ultimately allowed for prediction of long-term average $PM_{2.5}$ exposure at participant homes between 1978-2018 and individualized exposure averaging periods.(48)

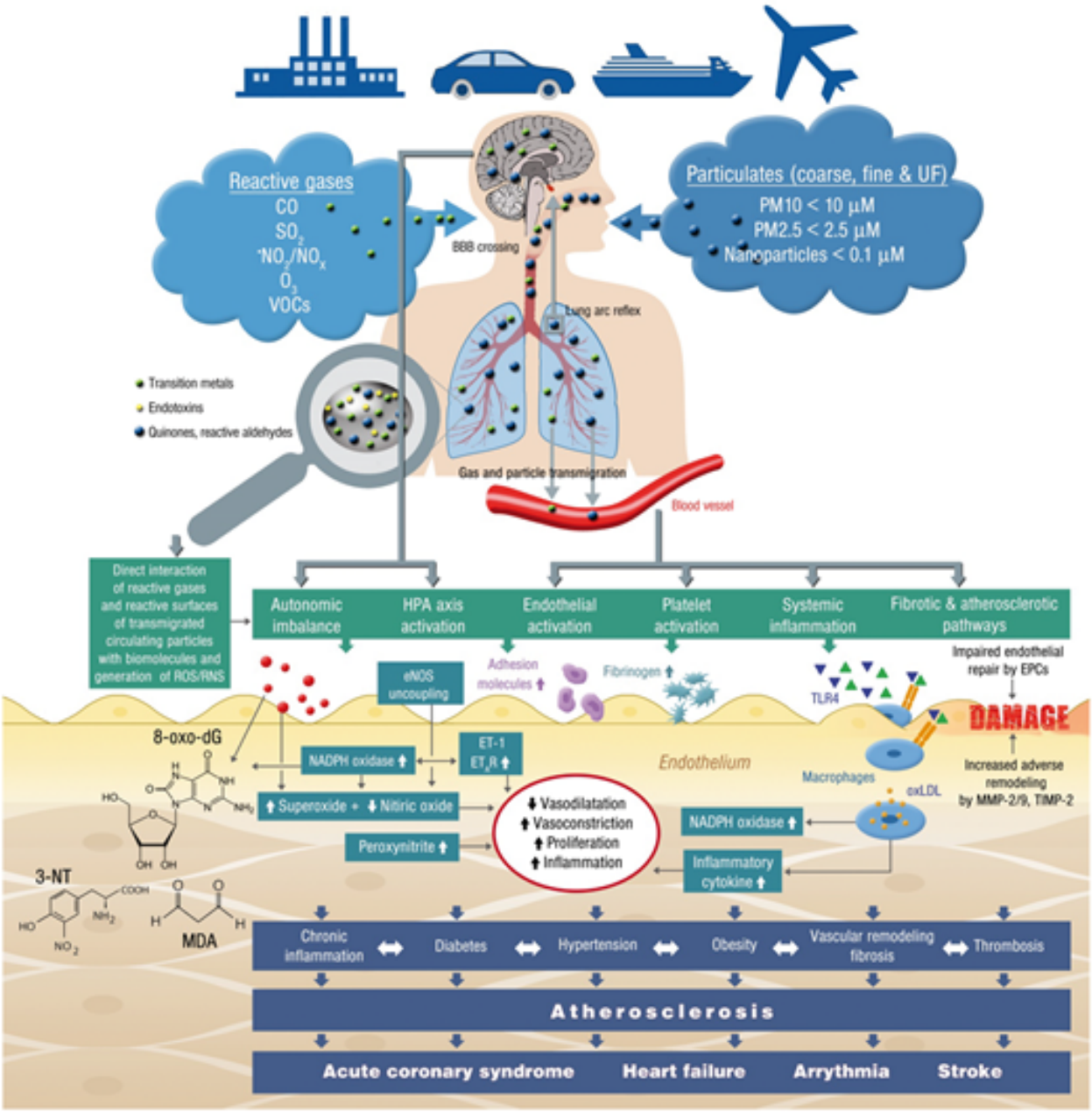

Figure 1.1. Summary of AP effects on Human health, specifically along the pulmonary and cardiovascular systems. AP gases and particulates interact with biological systems along numerous pathways, though primarily through induction of inflammation and subsequent cellular damage. Figure from Münzel et al and used per the creative commons license (creativecommons.org/licenses/by/4.0/) (23).

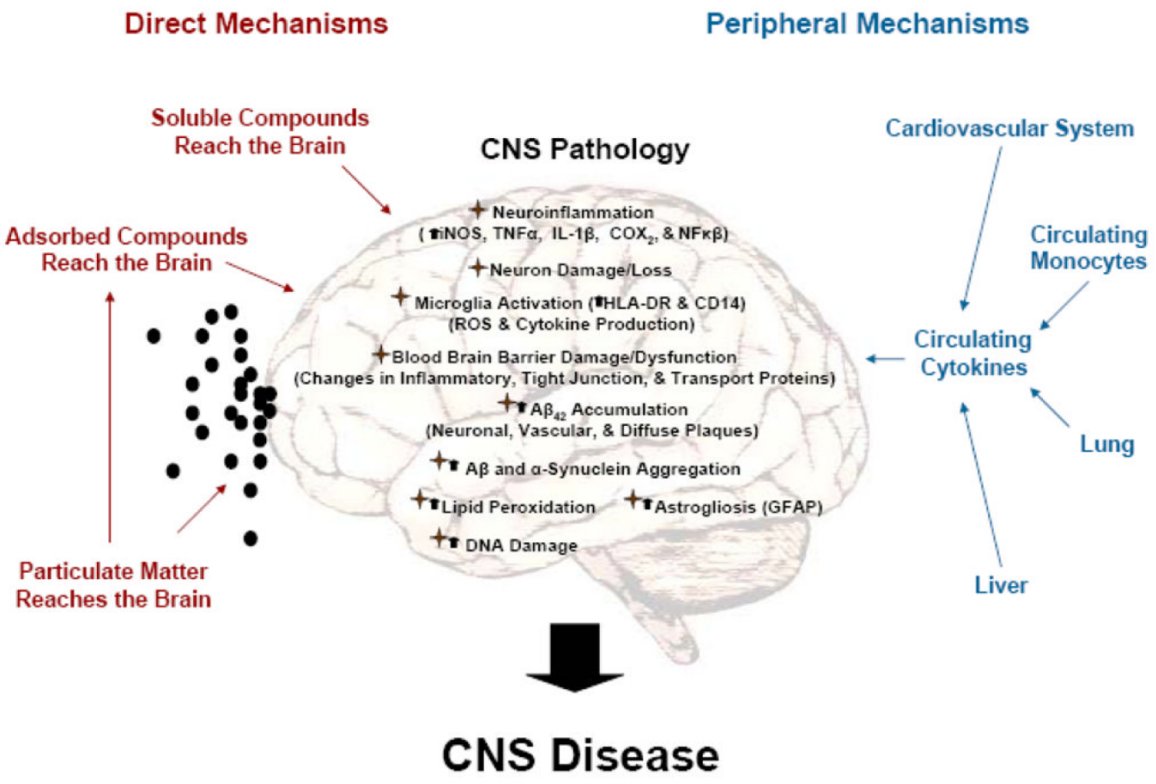

Figure 1.2. Illustration of the routes AP has been shown and/or theorized to impact neural tissues and contribute to the development of disease. The interactions are a complex series of events and compounds involved, but generally considered in four major groups: 1) Systemic inflammation; 2) Particulate Matter; 3) Adsorbed compounds; 4) Ozone. No single pathway to CNS damage has been definitively identified but believed to be better represented through a synergistic interaction of the pathways above. Figure adapted from Block et al. (22)

Chapter 2. METHODS

2.1 STUDY POPULATION AND SUBJECT SELECTION:

The Adult Changes in Thought (ACT) is a prospective, longitudinal, observational cohort study conducted in King County, Washington, consisting of a random sampling of individuals 65 years old and over who received medical care through a local health maintenance organization.(47, 51) Subjects are evaluated for onset of dementia and other degenerative diseases of cognition and included autopsy as an outcome for more in depth investigations. At the time of the start of our study, over 800 subjects had been autopsied and several secondary studies performed to investigate histological changes within the central nervous system (CNS) and potential relationships to a wide range of environmental exposures. The ACT-Air Pollution Study (ACT-AP) used existing ambient air pollution monitoring data and data from new, low-cost sensors to estimate individual level exposure to air pollution (including ultrafine particulate matter) at residential home addresses. To optimize our ability to identify pollutant particles in the brain, we selected those subjects having the highest estimated individual exposure over the 10 years prior to death.(48) Biopsy specimens were obtained from 11 subjects, specifically from the olfactory bulb (4 subjects), frontal lobe and cerebellum (11 subjects).

2.2 SAMPLE COLLECTION AND PREPARATION:

2.2.1 *Human brain tissue*

The brain biopsy tissue was harvested as part of the protocol autopsy and fixed with formalin for 2 weeks, then measured, photographed and examined for gross changes. Specimen blocks were then embedded in agar, cut to 4mm slabs using a meat slicer and further inspected through gross observation and image analysis. The slabs were then cutdown, placed in embedding cassettes and

processed using a standard automated paraffin embedding system. Microscopic specimens were sectioned from the cassette blocks after being chilled for 2 hours with ammonium hydroxide, cut on a microtome to 5 μm, floated onto a 40 - 45 °F waterbath and then mounted onto positively charged slides. The sections were left unstained, cover-slipped and sealed to maintain hydration of the tissue.

2.2.2 *Diesel Soot*

Diesel soot is a heterogeneous mixture of approximately 61% aciniform elemental carbon, 30% solvent organic fraction (SOF)/organic carbon, 8% sulfate and other chemicals and 1% metals.(52-54) Particulate matter from Diesel exhaust (DEP) was obtained from previous experiments which created controlled diesel exhaust atmospheres and filtered them through PTFE filter paper for additional testing using a 2002 model year turbocharged direct-injection 5.9-L Cummins, Inc. (Columbus, IN), B-series diesel engine (model 6BT5.9G6).(55) Material was stored in a sterile container for further study. Approximately 1 gram of particulate matter was provided for use and placed directly on a coverslip for imaging. Additional soot was used to generate several solutions of a known concentration in culture media and creation of a series of positive control specimens.

2.2.3 *Murine Alveolar macrophage uptake of soot.*

RAW 264.7 murine alveolar macrophage cells were grown on glass slides then exposed to concentrations of 0, 0.025, 0.05, 0.1, 0.25, 0.5, 1, and 2 ug DEP/mL culture media in culture media for 24 hrs. Cells were washed with PBS for 5 mins twice, then fixed for 15 minutes with 4% paraformaldehyde, washed again in PBS, cover-slipped and sealed with nail polish.

2.2.4 *Murine brain tissue*

Brain tissue was obtained from eight mice used in a parallel project to serve as additional positive and negative imaging controls, consisting of four naïve (wild type FA) and four diesel exhaust atmosphere (DE) exposed, 6 month old mice. The DE mice were exposed perinatally from gestation through postnatal day 21 to 300 $\mu g/m^3$ diesel particulate matter, 6 hours per day for 5 days per week. The mice were euthanized according to our institutional IACUC guidelines and the cranium incised. CNS tissues were fixed with a 4% formalin solution administered through cannulation of the circulatory system prior to removal from the cranium. Once harvested, the tissues were washed in PBS and then stored in sealed tubes containing PBS at 40° Fahrenheit.

The brains were sectioned by hand, first dividing the hemispheres along the midline using a disposable microtome sectioning blade. The left hemisphere was returned to the PBS storage for future use in another experiment. The right hemispheres were next serially sectioned in the sagittal plane using a commercially available stainless steel mouse brain matrix with 0.5 mm cutting guides and a new disposable microtome blade. Sectioning began from the lateral/temporal lobe and progressed medially, yielding 6 to 7 sections per subject. The sagittal plane was chosen so as to optimize the visibility of the olfactory bulb and tract tissue. Sections were secured on glass microscope slides, wetted with PBS, and coverslips applied. The slides remained in sealed petri dishes at 40°F until imaged.

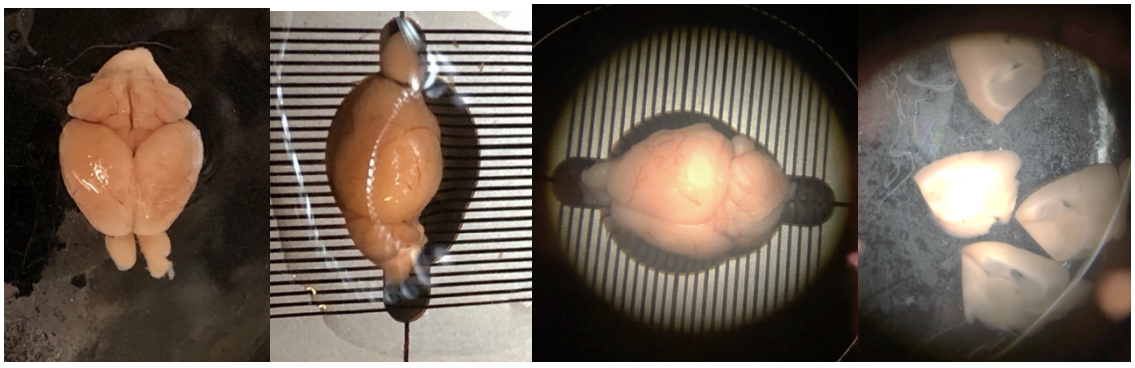

Figure 2.1. Mouse brain preparation. A) Freshly harvested and fixed. B) Using a commercial brain matrix for orientation and C) initial midline sectioning. D) Representative sagittal sections.

2.3 IMAGING PROTOCOL FOR BLACK CARBON DETECTION IN THE CENTRAL NERVOUS SYSTEM

2.3.1 *Microscopy*

This pilot study utilized a hyperspectral stimulated Raman scattering (hsSRS) microscope (Insight DS+ from Spectra-Physics) described in other publications.(38, 56, 57) The system uses a femtosecond dual beam laser system at an 80 MHz repetition rate: a tunable beam (pump), which ranges from 680 to 1300 nm, and a fixed beam (Stokes) at 1040 nm. The respective beams are chirped by a grating-based pulse stretcher. The laser is focused onto the samples through a 25X Olympus water immersion objective (Olympus, XLPN25XWMP2) with 1.05 NA, providing an average power of 30mW each. Backscattered light from the sample is collected by the excitation objective and reflected by a polarizing beam splitter (PBS). A quarter waveplate was placed between the PBS and the objective to produce circularly polarized light to be focused on the photodiode. Images are generated via Raster scanning of the laser focus over the sample, consisting of 512x512 pixels with an 8 μs/pixel dwell time (frame rate 0.5 frame/s). The backscatter and SRS signal filtering is performed through use of either a 600 nm short pass (macrophages) or 550/80 nm (CNS tissues) bandpass filter between the objective and photodiode. The hyperspectral SRS signal was detected using a lock-in amplifier. Overall, image resolution was ~ 0.5 μm and spectral resolution ~ 12 cm^{-1}. Stage control and image acquisition was controlled via a graphical user interface coded in Matlab. See Figure 2.2 for a graphical representation of the system as described in Figueroa et al. 2019.(56) Data was saved with relative intensities in arbitrary units (a.u.) over the wavenumber region of 2800 to 3100 cm^{-1} (C-H stretching). A single human sample was also

looked at in the fingerprint region of 1500 – 1700 cm^{-1} to attempt chemical isolation of the background and carbon particulates following modification of the microscope to shift the available RAMAN spectra.

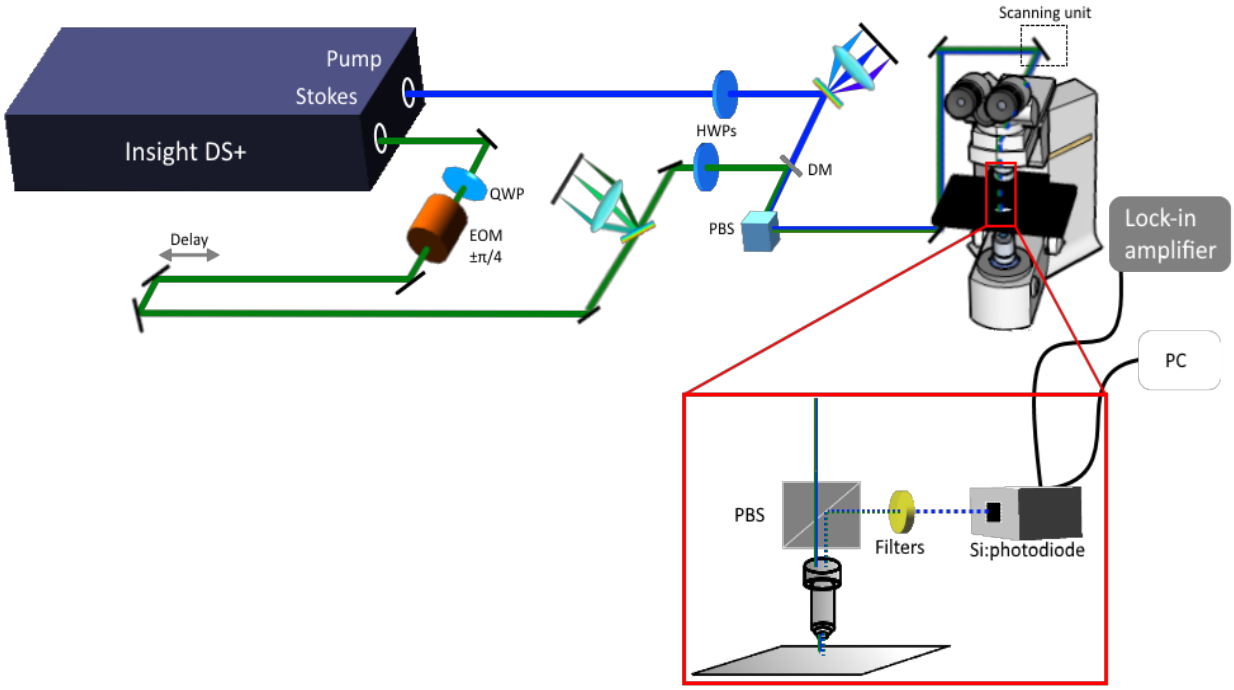

Figure 2.2. Diagram from Figueroa et al 2019. Schematic of the hsSRS microscope based on a femtosecond dual beam laser system. Abbreviations: QWP, quarter waveplate; EOM, electro-optical modulator; HWP, half waveplate; PBS, polarizing beam splitter; DM, dichroic mirror; SPF, short–pass filter; PD, photodiode.(55).

2.3.1.1 Diesel soot and murine DEP exposed macrophage

Each specimen was imaged using a larger Raster pattern of 20 frames, using a 600nm short pass filter and covering a field of view of 270 x 270 μm^2 for each frame. Three frames were also imaged in the z-direction to investigate the 3-dimensional structure of the cells and particulate location. Images were saved into TIFF files containing the interleaved SRS and fluorescent images.

2.3.1.2 Mouse brain imaging

Samples were imaged in a similar Raster pattern of 8x8, 14x14, 16x16 out to 66x22 frames, covering a field of view of 180 x 180 μm^2 to scan as much of the tissue as possible and optimize the search area for particulate matter. This imaging also allowed for fine tuning of the imaging parameters to be used for the human specimens.

2.3.2 *Human subject imaging*

Using the imaging parameters identified from the mouse brain imaging, the human sections were then imaged, starting with sections identified as originating from the olfactory bulb, followed by sections from the frontal lobe and cerebellar blocks. These were similarly taken in a step-wise Raster pattern.

2.3.3 *Image analysis*

2.3.3.1 Software:

Images were manipulated and processed using FIJI/ImageJ, an open-source image processing software package initially developed by the NIH. The standard installation package for FIJI were used for the primary image processing and analysis.

2.3.3.2 Image preparation

The SRS and fluorescence channel were deinterleaved for all images investigated and processed separately. For specimens imaged across multiple fields of view in a sequential tiled fashion, reconstruction of the scanned surface was performed by stitching of the image tiles using the Grid/collection stitching plug-in described by Preibisch et al 2009.(58) Images to be subjected to thresholding analysis were converted to 8-bit TIFF format and saved in separate files from the original raw data.

2.3.3.3 Alveolar Macrophage analysis

Two to three frames from the 20 taken for each DEP exposure concentration were selected at random and used to identify a dose-response relationship between exposure and macrophage

uptake of particulates. The individual cells were identified in each SRS frame and the corresponding particulates in the fluorescence frames. Area measurements of DEP relative to the macrophage cells were obtained and correlation calculated.

The SRS images were optimized in brightness and contrast levels to identify cell edges and other structures using the automatic adjustment available in FIJI. Threshold processing was then performed to identify the cell body edges and allow for measurements to be taken. Thresholding utilized the mean pixel algorithm,(59) followed by pixel smoothing and conversion of the images to a binary format. Individual cells were identified using the *Analyze particles* function, selecting areas of 50-550 μm^2 as the anticipated size range of the macrophages based upon available literature reports for murine alveolar cells.(60, 61) Measurements were obtained for the area and saved to a *.csv* file. The image ROIs were color coded green for later overlay with the DEP identified image.

The fluorescence images were used to identify DEP through a similar thresholding process. Previous studies using two photon femtosecond pulsed laser at 810nm illumination have established carbon black particles produce a broad band white light (WL) stretching over the entire visible light spectrum at high intensity.(35, 62, 63) Images of the pure diesel soot images revealed heterogeneous particles with high intensity fluorescent signals within them and this became the primary area of interest for the particulate analysis.

Thresholding of the particulate fluorescence was performed with the Otsu algorithm,(64) followed by pixel smoothing and saving as a binary image. Particulate area was measured using the *Analyze Particles* command, selecting between 1-900 μm^2 as we anticipated there would be wide variability in the size distribution of the particulate aggregates present within the cells.

Measurement data was saved to a *.csv* file and ROIs used to generate a red color-coded overlay for localization within the identified cells in the earlier step.

The overlays were used to match the measured cell and particulate areas to determine the percent area of the cell occupied by the DEP. Cells and particulates without a counterpart were not included in the calculations. Similarly, paired measurements where the particulate area was larger than the corresponding cell area were considered to reflect cellular destruction and disregarded in the percent cellular area calculations. The individual percent cellular areas of DEP were plotted versus their respective DEP exposure concentrations and correlation calculations performed. The average percent cell area of DEP was also determined for each frame and a scatter plot of these versus the exposure DEP concentration generated. A linear trend line and Pearson's correlation coefficient was calculated.

2.3.3.4 Mouse brain analysis

Image tiles were deinterleaved and stitched together as previously described. The SRS channel tiled image was then thresholded and intensity detection performed with a focus along the olfactory bulb and tract for the naïve and DE subjects. Control and DE images were compared to identify areas for potential particulate matter isolation.

2.3.3.5 Human CNS tissue analysis

Image tiles were deinterleaved and stitched together as previously described. Image contrast and brightness of the SRS images were further optimized to distinguish between suspected BC aggregates and the surrounding embedding medium. Secondary images of one of the biopsy slides of an olfactory bulb region were also taken in the fingerprint region to better characterize the chemical RAMAN spectra to attempt to isolate a BC signal from the background.

Tissue concentration of particulate matter would be determined by random sampling along the identified tissue structures of 10 circular ROIs with a diameter of 20 μm. Areas with WL saturation would be measured and to determine whether the particulates were intra or extracellular. If several regions of the brain tissues were identified as containing particulate matter, separate average areas of particulates were determined, and approximate concentration estimated for each region based upon relative area occupied.

2.4 AMBIENT AIR POLLUTION EXPOSURE MODELING

Estimated individual exposure to ambient $PM_{2.5}$ and NO_2 at the residential home address was determined previously using a novel spatio-temporal modeling system based upon extensive regulatory and low-cost sensor data obtained throughout the Puget Sound as previously described.(48) Published model data focused on the 10 year period prior to death and autopsy. This data was initially used to select the subjects from the ACT study with the highest estimated ambient exposures to facilitate the identification of BC in the CNS tissues.

2.5 STATISTICS:

2.5.1 *Descriptive statistics and Pearson's correlation coefficient calculation for diesel soot controls*

Macrophage uptake data consisted of quantification of the number of cells per ROI/frame, the corresponding area of each cell, major and minor axis lengths, and the mean pixel intensity ± standard deviation. Primary analysis was undertaken to establish a dose response relationship between the DE incubation solution concentrations and macrophage uptake of DEP. The mean cellular area was calculated from five frames sampled at each concentration. Particulate area was measured in five randomly selected cells for each frame, ignoring signal elements falling outside or on the continuous edge of the sample cells. The ratio of DEP area relative to the cellular area

was calculated and the mean ± standard deviation were calculated for the cell areas, particulate areas and relative percent area. A scatter plot of the area ratio versus the DEP concentration were created and overlapping linear correlation line with 95% CI using R Studio. Pearson's correlation coefficient was calculated for the correlation between the concentration of incubated DE and ratio of DEP area to cellular area.

2.5.2 *Descriptive statistics and Linear regression model for human subject data*

Images were scanned via intensity thresholding and relative area of potential particulate matter marked and calculated. The location of the particulate matter (intracellular versus interstitial) would determine additional quantitative analysis. If particulate matter was found to aggregate or be intracellular, the relative cellular area would be calculated for 5-10 ROIs and basic descriptive statistics determined.

Quantified particulate matter from brain biopsy data would then be compared to available individual air pollution exposure estimates at the residential home address and rough fit using Pearson's correlation coefficient.

Chapter 3. RESULTS

3.1 DIESEL SOOT AND ALVEOLAR MACROPHAGES

A linear dose-response relationship was identified between macrophage uptake of DEP and the incubation exposure concentration of DEP. (Figure 3.1) With increasing DEP concentration, there was a positive trend in the mean area of DEP associated with identified cells, relative to the individual cell areas. It was also noted that the total number of cells within the sampled section determined to contain DEP increased with the increasing inoculation concentrations (data not shown). Cellular structures, particularly the plasma membrane and nuclei, were less identifiable with increased concentration. The amount of DEP not associated with cells was highly variable with a trending increase at higher concentrations.

The sampled data points were analyzed in R Studio. A Pearson's correlation test was performed using the raw data as seen in Figure 3.1, with an overlying regression line and 95% confidence interval. The box plot better illustrates the variability in cell data as well as the increasing trend in means. Table 3.1 provides the mean cell areas and ratio of DEP area to cell area for each concentration of DEP used in the exposure testing.

Table 3.1: Alveolar Macrophage uptake of DEP following incubation over 24 hours at increasing concentrations of DEP. There appears to be a transition point around 0.2 µg/mL where the macrophages take up DEP more readily as well as an upper limit of material the cells are able to engulf before succumbing to the toxicity of the DEP.

DEP incubation concentration (µg/mL media)	DEP cells/total cells (%)	Mean DEP/cell area % (SD)	Cell area mean um^2 (SD)
0	0	0 (0)	320.1 (210.4)
0.025	79/305 (26)	2.6 (4.6)	490.9 (252.5)
0.05	58/215 (27)	1.4 (1.8)	485.4 (263.5)
0.1	45/196 (23)	9.4 (15.4)	266.5 (169.8)
0.25	99/127 (78)	18.1 (12.3)	247.9 (220.0)
0.5	121/159 (76)	16.5 (14.6)	264.3 (169.6)
1	74/133 (56)	18.1 (15.7)	183.6 (145.1)
2	274/278 (99)	40.1 (24.8)	487.5 (589.1)

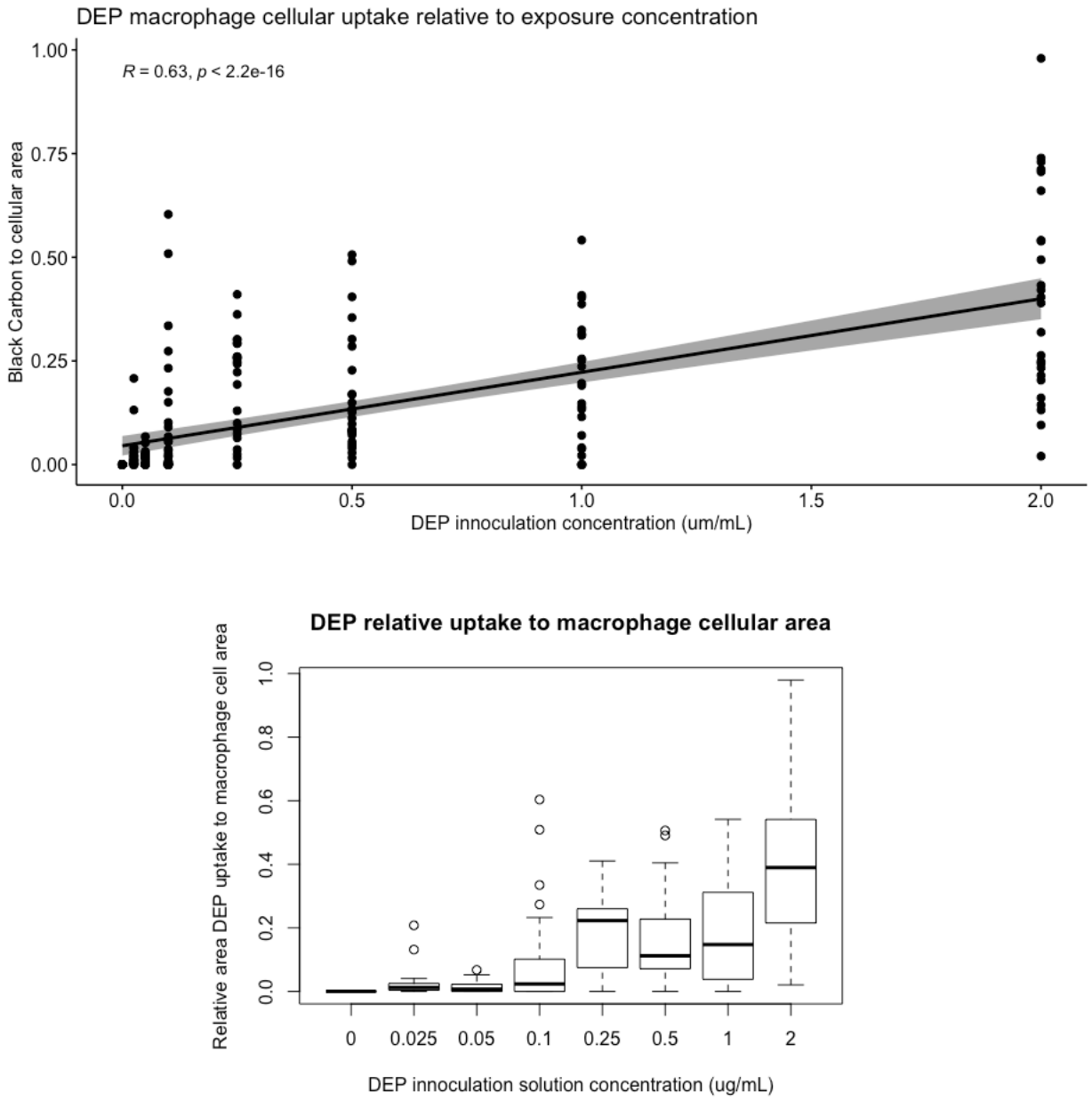

Figure 3.1. Individual and averaged data points for particulate uptake by the macrophages expressed as the relative area of DEP to the area of the cells containing DEP. There was significant variation in DEP uptake among the sampled cells at each DEP concentration both in terms of the total number of cells identified with DEP uptake and total particulate uptake. Overall, exposure to increasing concentrations of DEP were associated with increasing macrophage uptake of DEP, as indicated by a linear, positive correlation (R=0.63, p value < 2.2e-16).

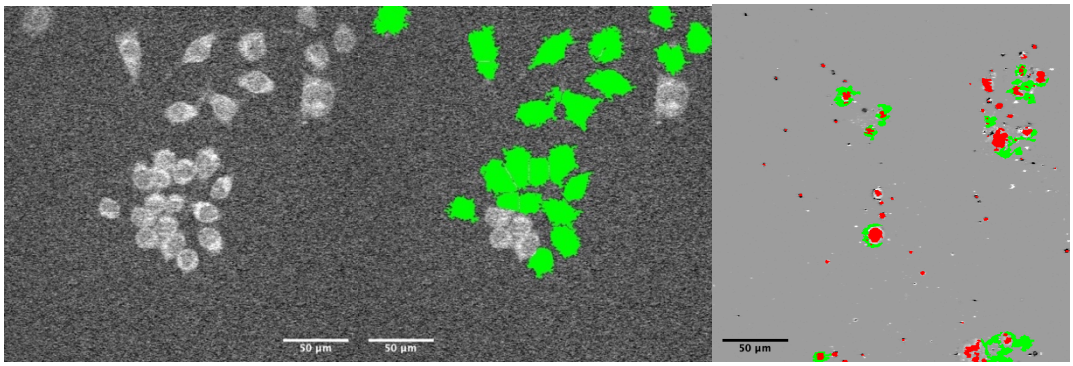

Figure 3.2. Representative image thresholding procedure for cellular and particulate identification and area measurements. Unexposed macrophage cells (left) and 0.1 ug DEP/ml media (far right). Cell outlines were more readily identified without exposure to DEP. Green areas correspond to macrophage cell areas as determined through threshold and edge analysis of the SRS images. Red areas correspond to DEP matter as determined through signal intensity thresholding of the fluorescence channel. The underlying gray scale image is from the SRS channel used as the base for cell identification and measurement.

3.2 Mouse CNS Tissue Imaging

Comparison of 3 pairs of the naïve and diesel exhaust exposed mouse specimens did not identify regions of potential particulate collection, though several larger structures and cells were identifiable. Image scan collection was complicated by the non-parallel cut tissue surfaces "falling" out of the focal plane as the target was moved. There were occasional data collection errors leading to "lost" tiles within the sequences complicating reconstructing the entire surface for broader image analysis.

As seen in Figure 3.3, the most identifiable structures within the brain sections tended to be vascular areas, particularly when red blood cells remained within the larger vessels. Axonal elements and larger collections of cells were readily identified as brighter and darker signal

intensities, respectively. Microglial cells or areas of protein accumulation were not readily identified in the DEP exposed brain tissues when compared to the naïve specimens.

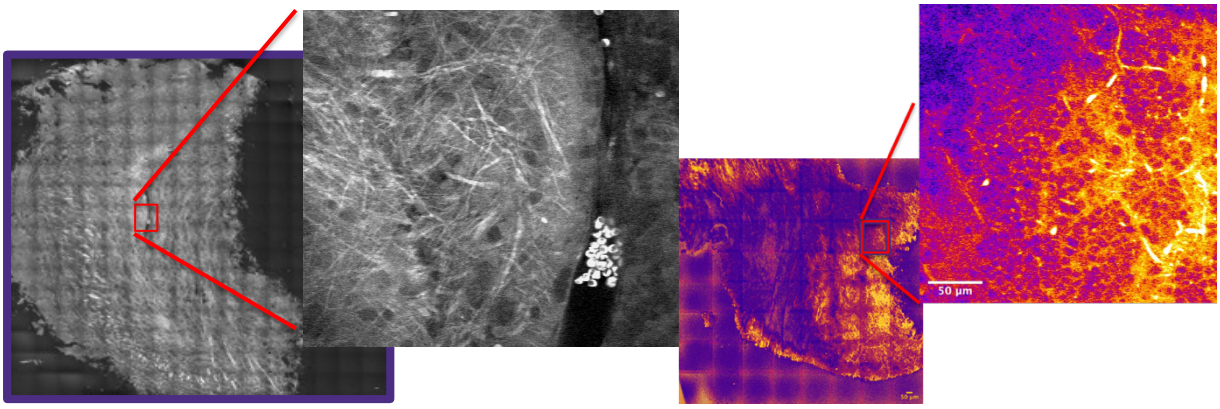

Figure 3.3. SRS images of naïve (left) and DE exposed (right) mouse neural tissue. Several structures were identifiable in the thicker tissues, specifically the axonal distributions seen as brighter fibrillar elements and residual red blood cells located within the vessels of the brain (left inset/zoomed image). The DE exposed tissues on the right appear more cellular, though image resolution was reduced due to noise in the system and variation in the tissue surface smoothness requiring alterations in the scan setup.

3.3 HUMAN CNS IMAGING

The human specimen imaging was complicated by numerous issues, including section thickness and unexpected tissue mounting media. Observational analysis of the images suggested few structures were readily identifiable and secondary imaging through either brightfield or light microscopy was not readily available to provide assistance in gross structural identifications. Individual cells were the most commonly identified landmarks, though cell type identification was not possible. Signal intensity differences of cellular and extracellular objects were essentially uniform throughout the spectral ranges scanned. Representative slides from the olfactory bulb were also examined in the fingerprint spectral region, in an effort to determine whether the background signal might be removed or otherwise separated from the tissue and/or particulate signals.

Representative SRS and Fluorescence images from a cerebellar region biopsy are presented in Figure 3.4. Compared to images available from pathology and anatomy resources, the cellular configurations are similar to the granular layer interface within the cerebellum. Figure 3.5 and Figure 3.6 are representative images from the frontal lobe and olfactory bulb, respectively.

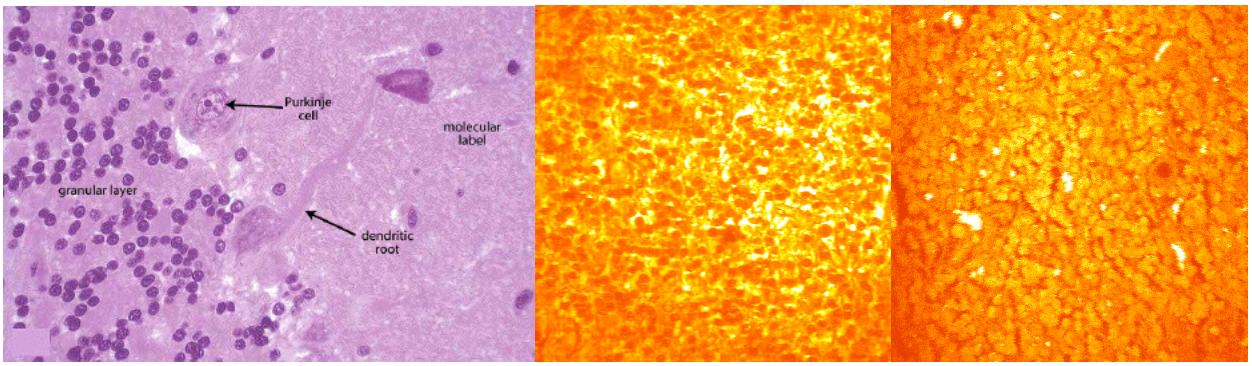

Figure 3.4. Cerebellar section imaging. A) H&E stained section at the interface of the gray matter and granular cells. B) SRS image at second wave number peak, from the granular layer. C) Corresponding Fluorescence image. H&E image downloaded from: https://www.dartmouth.edu/~anatomy/Histo/lab_3/neuro/DMS098/popup.html

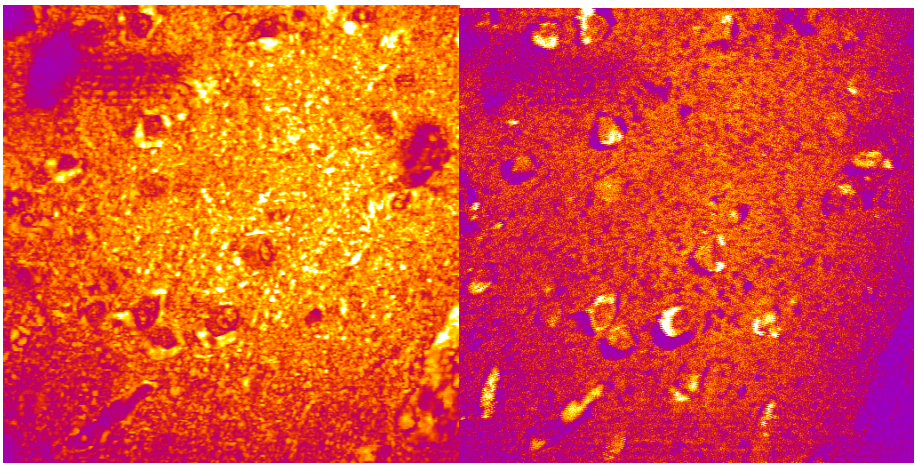

Figure 3.5. Frontal lobe section imaging. A) SRS image with rough cellular borders visible; B) Corresponding Fluorescence image. Axonal elements were less obvious throughout these regions and areas of potential particulate related signal not readily separated from the surrounding background.

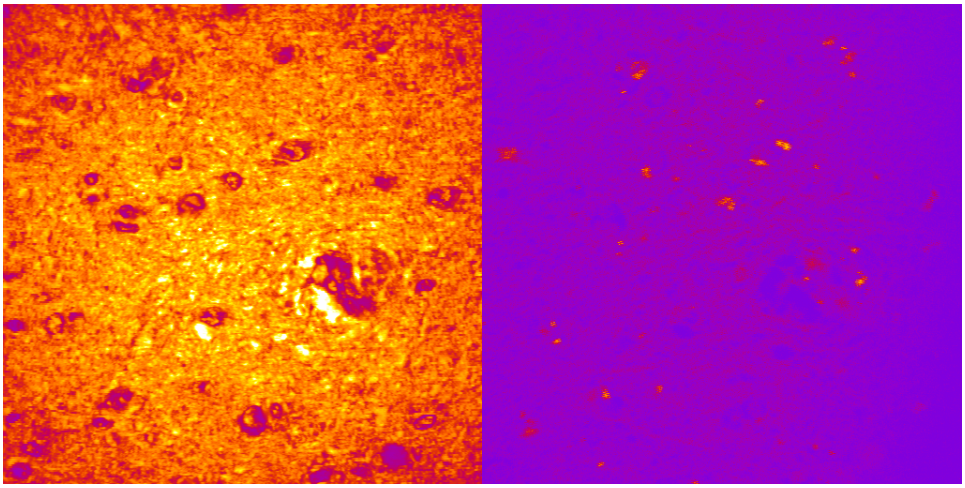

Figure 3.6. Olfactory bulb section imaging through the fingerprint RAMAN spectral region. A) SRS image at the “G” peak. B) Corresponding Fluorescence image. Gross cellular structure is visualized again without obvious particulate matter and autofluorescence in B appears mostly associated with nuclear structures of the visible cells.

Chapter 4. DISCUSSION

Our study successfully identified a positive dose response association with DEP exposure and the subsequent uptake of material in mouse alveolar macrophages *in vitro* using SRS microscopy. Our goal of identifying pollutant particles in brain tissue from both mouse and human subjects with known and estimated exposures to air pollution was not successful and we were unable to attempt to develop a dose response regression model.

The ability of AP ultrafine particles to penetrate highly protected and critical organ systems has been theorized and demonstrated in several studies using a variety of techniques.(27, 35, 62, 63, 65) Our study sought to capitalize upon those findings using a similar imaging system and access to neural tissues from a large cohort of subjects with established individual PM exposure estimates over at least a decade. We have demonstrated that this technique is a feasible approach to identifying particulate matter, despite the difficulties in the actual execution of the imaging.

Our initial study looking at how the DEP would present in the SRS and Fluorescence imaging compared favorably with earlier studies identifying black carbon in fetal tissues.(63) In that study, the investigators were able to establish an approximate environmental exposure for the pregnant mothers over the course of their pregnancies and correlate the particulate matter detected using their two photon system, which was technically similar to ours. While their study also utilized TEM to better establish particle concentrations in the tissues as well as particle sizes, we were able to identify a similar signal intensity of the DEP to excitation by the laser via the fluorescence detection channel, providing additional support that particulate matter in our study should respond similarly within the neural tissue samples, if present in adequate concentration.

The observation of significant morphological changes evident in the detected macrophage cells was expected, though there was considerably more extracellular DEP material than

anticipated, suggesting either incomplete washing away of the inoculation solutions, surface adsorption of the particulates to the cells or compromise of the cell integrity. At the lower concentrations of DEP, it would seem reasonable to assume there was an electrostatic interaction between the particulate matter and the glass slides used as a base to hold and inoculate the macrophages, since such microscope slides are positively charged to improve tissue section adherence. In the absence of additional imaging verification, the issue of surface versus intracellular particulate matter is more difficult to address. A single set of cells exposed to 0.1 μg/mL DEP were examined quickly under brightfield microscopy, showing the material to likely be contained within endosomes or lysosomes of the macrophages, but confirmatory membrane labelling antibodies were not available. At the higher concentrations of DEP (over 0.5 μg/mL), the appearance of smaller cellular areas and DEP signal areas overlapping or otherwise covering the cell edges was concerning for ongoing cell damage and death versus combined intracellular and extracellular processes. Additional imaging such as transmission or scanning electron microscopy would help to better distinguish between such options in future studies.

Our decision to further investigate the potential deposition routes and ultimate localization of black carbon within the brain was driven by numerous studies identifying iron,(30) magnetite(28) and other AP associated metals in animal and human neural tissues.(25) Each of these studies identified a strong correlation with exposure to nanoparticulates and possible transport routes into the brain tissues, specifically through the olfactory tract and systemic circulation. Those findings supported our effort to use naïve and DE exposed mice available from a sister project, in an effort to similarly identify possible particulate concentrations and a transportation related gradient of material towards the brain.

There are several potential reasons that we were unable to identify particles in murine CNS samples. Possible technical explanations include inadequate microscope resolution (our system was ~ 0.5 μm), inappropriate sample preparation or sampling error. Alternatively, there is the possibility the black carbon particles either do not reach the brain over the study time period or are cleared from the CNS over time. Prior studies have predominantly looked for heavy metal deposition and/or transport in the CNS, with the assumption of their association with pollutant exposure. We are unaware of any studies investigating the longevity of the black carbon cores *in vitro* or *in vivo*, though could consider a secondary analysis trying to identify the metallic components associated with the DE used in the murine study in future experiments.

The subject mice used in this portion of the study had only been exposed perinatally up to 3 weeks postnatally. As sacrifice occurred at age 6 months and we have no data related to whether the DE particulate matter ever entered the brain tissue, it is possible there were no particles to identify, either through clearance by the immune cells or more effective blockage of particulate translocation than seen in other studies. There currently is no literature available suggesting the microglia and other innate immunity scavenger cells would be capable of clearing PM from the brain parenchyma and over what time frame. The images capturing intact intravascular red cells suggest we may be able to better determine the intracellular vs extracellular nature of DEP/black carbon with adsorbed metals, though the concentration of iron in the red cells is more uniformly distributed than anticipated particulate matter engulfed or otherwise taken up by cells. Future rodent studies may be better structured to sample tissues a several points during exposure as well as following the cessation of exposure so as to determine the natural history course of particulate entry and clearance within the brain.

Given the difficulty in obtaining uniformly thick brain tissue sections for imaging, the most likely scenario is that we were not able to maintain adequate resolution throughout the scanning process, either due to tissues moving out of the focal plane or introduction of other unaccounted for variables. These would all influence our ultimate resolution capability. Examination of the images under greater magnification revealed several areas of consistently bright signals along some cells and other structures, though limited to one or two pixels and likely more representative of noise. Increasing the number of specimens, using a repeatable tissue sectioning process and more than a single removed exposure timepoint would provide more reliable data for future investigations. Incorporation of additional imaging processes such as TEM would also serve to address the question of particle size detection as well as relationship to the cells, though the required solvents in the tissue processing may remove molecules and other particles of interest.

Our primary objective of identifying black carbon particles in human brain tissue using SRS microscopy was ultimately unsuccessful, though still provides useful information for future investigations. Of greatest utility, would be an investigation using a more sequential imaging technique sequence for data comparison, specifically obtaining fresh fixed brain biopsy tissue, optimizing tissue thickness for SRS microscopy, followed by further division of the tissue and sectioning for light and TEM. Technically, it is challenging to ensure imaging of the same regions through such a range of tissue processing requirements and would require some form of coordinate registration system to maintain the potential for image comparisons. Continued advancements in the resolution and acquisition speed of SRS microscopy are encouraging for the future ability to detect ultrafine particulates in tissues.(37) The difficulties we encountered in attempts to distinguish the background signal from possible particulates in the tissues have served to better define future endeavors and utilize several modalities to support the investigation.

Other investigators using RAMAN microscopy techniques to identify neural anatomy, degenerative changes and cellular metabolic processes have prompted the development of commercial labels, more standardized equipment and experimentation with finer resolution capability. The scientific excitement to further explore the capabilities of these tools is likely to continue driving the refinement of techniques and equipment for many more years.

This study sought to utilize stimulated Raman scattering microscopy to identify black carbon particulate matter in the CNS tissue of human subjects with estimated high individual exposures to AP ultrafine particulate matter. Initial assessment of positive control specimens with known concentration exposures to DEP was encouraging for the ability to distinguish a dose response relationship in cellular uptake utilizing SRS imaging techniques. Imaging of murine brain tissue revealed larger axonal or tract structures, though nanoparticles were not identified in any of the locations investigated. Whether this was due to limited concentration of BC below the imaging resolution of the microscope, a lack of olfactory bulb/tract PM uptake or clearance of neural PM by immune surveillance cells in the four months following last exposure is not able to be determined with the current level of data. A separate targeted study may help to better answer those questions in the future.

Chapter 5. LIMITATIONS AND FUTURE WORK

5.1 LIMITATIONS

The primary limitations of our study lay in the lack of a consistent and uniform approach to the preparation and handling of the various specimens utilized throughout the study. The human specimens were obtained in a form allowing for future, more traditional microscopic investigations to be performed, leading to complications with the presence of paraffin and not enough tissue to provide enough identifiable structure under the SRS imaging. The mouse brain specimens were the most useful, from the structural imaging sense, though had similar processing complications due to equipment pending repair and the need to section the brains by hand. The alveolar macrophage cells from culture may also have introduced another variable in terms of potential differences in activity *in vitro* versus *in vivo.*

The resolution of the current imaging system is not fine enough to identify non-aggregate ultrafine particulate matter in bulk tissues, though the concentration exposure study showed it to be appropriate with aggregate materials. Bové et al(63) demonstrated black carbon particulate detection in fetal tissues at approximately 1 μm in diameter, which suggests the particulates are prone to at least some aggregation *in vivo* and detectable using our microscope.

As mentioned previously, the clearance rate of PM from neural tissues, or lack thereof, remains an unknown variable in this study. Other studies linking the presence of particulate matter with the development of local inflammatory reactions and uptake by periglomerular neurons and erythrocytes suggest the particulates are prone to uptake by non-immune cells, which may protect them from clearance if not immediately toxic to the cell and contributing to its death.(22)

Finally, not having a "gold standard" technique of confirming the presence of the particulate matter in the brain tissues left us without the ability to further trouble shoot the SRS imaging and answering the question whether the particles were present at all. This was considered and will be utilized in future, following reopening of resources as the pandemic evolves.

5.2 FUTURE WORK

Additional opportunities for the future include the incorporation of commercially available carbon black as a positive control as it has become a widely accepted surrogate to black carbon due to the ability to maintain a more homogeneous size, contains a higher amount of pure carbon and has a well characterized RAMAN spectrum. This would allow for additional cultured cell exposure experimentation and uptake correlations, particularly if able to look specifically at the activity of microglial cells, macrophages, astrocytes and oligodendrocytes in response to increasing exposure concentrations.

Finally, conducting a larger mouse exposure study with multiple tissue sampling time points throughout the exposure period and beyond would provide insights into the longevity of DEP and other nanoparticles in the CNS. Such a study may also provide insights as to changes in the inflammatory response of the involved tissues and production of associated degenerative proteins. Additionally, if a dose response can be estimated based upon exposures in the mouse model, future human studies should be similarly successful and such models could become a useful standard for assessment and estimation of air pollution exposures for subjects without the availability of regional environmental sampling data.

BIBLIOGRAPHY

1. Cohen AJ, Brauer M, Burnett R, Anderson HR, Frostad J, Estep K, et al. Estimates and 25-year trends of the global burden of disease attributable to ambient air pollution: an analysis of data from the Global Burden of Diseases Study 2015. Lancet. 2017;389(10082):1907-18. Epub 2017/04/10. doi: 10.1016/S0140-6736(17)30505-6. PubMed PMID: 28408086; PubMed Central PMCID: PMC5439030.

2. Nel A. Atmosphere. Air pollution-related illness: effects of particles. Science. 2005;308(5723):804-6. doi: 10.1126/science.1108752. PubMed PMID: 15879201.

3. Dockery DW, Pope CA, Xu X, Spengler JD, Ware JH, Fay ME, et al. An association between air pollution and mortality in six U.S. cities. N Engl J Med. 1993;329(24):1753-9. doi: 10.1056/NEJM199312093292401. PubMed PMID: 8179653.

4. Laden F, Schwartz J, Speizer FE, Dockery DW. Reduction in fine particulate air pollution and mortality: Extended follow-up of the Harvard Six Cities study. Am J Respir Crit Care Med. 2006;173(6):667-72. Epub 2006/01/19. doi: 10.1164/rccm.200503-443OC. PubMed PMID: 16424447; PubMed Central PMCID: PMC2662950.

5. Jerrett M, Burnett RT, Ma R, Pope CA, Krewski D, Newbold KB, et al. Spatial analysis of air pollution and mortality in Los Angeles. Epidemiology. 2005;16(6):727-36. doi: 10.1097/01.ede.0000181630.15826.7d. PubMed PMID: 16222161.

6. Pope CA, Burnett RT, Thun MJ, Calle EE, Krewski D, Ito K, et al. Lung cancer, cardiopulmonary mortality, and long-term exposure to fine particulate air pollution. JAMA. 2002;287(9):1132-41. doi: 10.1001/jama.287.9.1132. PubMed PMID: 11879110; PubMed Central PMCID: PMC4037163.

7. Miller KA, Siscovick DS, Sheppard L, Shepherd K, Sullivan JH, Anderson GL, et al. Long-term exposure to air pollution and incidence of cardiovascular events in women. N Engl J Med. 2007;356(5):447-58. doi: 10.1056/NEJMoa054409. PubMed PMID: 17267905.

8. Van Hee VC, Adar SD, Szpiro AA, Barr RG, Bluemke DA, Diez Roux AV, et al. Exposure to traffic and left ventricular mass and function: the Multi-Ethnic Study of Atherosclerosis. Am J Respir Crit Care Med. 2009;179(9):827-34. Epub 2009/01/22. doi: 10.1164/rccm.200808-1344OC. PubMed PMID: 19164703; PubMed Central PMCID: PMC2675567.

9. Wellenius GA, Burger MR, Coull BA, Schwartz J, Suh HH, Koutrakis P, et al. Ambient air pollution and the risk of acute ischemic stroke. Arch Intern Med. 2012;172(3):229-34. doi: 10.1001/archinternmed.2011.732. PubMed PMID: 22332153; PubMed Central PMCID: PMC3639313.

10. Fox MA, Tran NL, Groopman JD, Burke TA. Toxicological resources for cumulative risk: an example with hazardous air pollutants. Regul Toxicol Pharmacol. 2004;40(3):305-11. doi: 10.1016/j.yrtph.2004.07.008. PubMed PMID: 15546684.

11. Block ML, Elder A, Auten RL, Bilbo SD, Chen H, Chen JC, et al. The outdoor air pollution and brain health workshop. Neurotoxicology. 2012;33(5):972-84. Epub 2012/09/05. doi: 10.1016/j.neuro.2012.08.014. PubMed PMID: 22981845; PubMed Central PMCID: PMC3726250.

12. Ailshire JA, Crimmins EM. Fine particulate matter air pollution and cognitive function among older US adults. Am J Epidemiol. 2014;180(4):359-66. Epub 2014/06/24. doi: 10.1093/aje/kwu155. PubMed PMID: 24966214; PubMed Central PMCID: PMC4128773.

13. Allen JL, Liu X, Weston D, Prince L, Oberdörster G, Finkelstein JN, et al. Developmental exposure to concentrated ambient ultrafine particulate matter air pollution in mice results in persistent and sex-dependent behavioral neurotoxicity and glial activation. Toxicol Sci. 2014;140(1):160-78. Epub 2014/04/01. doi: 10.1093/toxsci/kfu059. PubMed PMID: 24690596; PubMed Central PMCID: PMC4081635.

14. Calderón-Garcidueñas L, Azzarelli B, Acuna H, Garcia R, Gambling TM, Osnaya N, et al. Air pollution and brain damage. Toxicol Pathol. 2002;30(3):373-89. doi: 10.1080/01926230252929954. PubMed PMID: 12051555.

15. Calderón-Garcidueñas L, González-Maciel A, Kulesza RJ, González-González LO, Reynoso-Robles R, Mukherjee PS, et al. Air Pollution, Combustion and Friction Derived Nanoparticles, and Alzheimer's Disease in Urban Children and Young Adults. J Alzheimers Dis. 2019;70(2):343-60. doi: 10.3233/JAD-190331. PubMed PMID: 31256139.

16. Cory-Slechta DA, Sobolewski M, Marvin E, Conrad K, Merrill A, Anderson T, et al. The Impact of Inhaled Ambient Ultrafine Particulate Matter on Developing Brain: Potential Importance of Elemental Contaminants. Toxicol Pathol. 2019;47(8):976-92. Epub 2019/10/14. doi: 10.1177/0192623319878400. PubMed PMID: 31610749; PubMed Central PMCID: PMC6911038.

17. Semmens EOB, Kaufman JD. Effects of traffic-related air pollution on cognitive function, dementia risk, and brain MRI findings in the cardiovascular health study 2012. Available from: http://hdl.handle.net/1773/21903.

18. Pun VC, Kazemiparkouhi F, Manjourides J, Suh HH. Long-Term PM2.5 Exposure and Respiratory, Cancer, and Cardiovascular Mortality in Older US Adults. Am J Epidemiol. 2017;186(8):961-9. doi: 10.1093/aje/kwx166. PubMed PMID: 28541385; PubMed Central PMCID: PMC6915823.

19. Shou Y, Huang Y, Zhu X, Liu C, Hu Y, Wang H. A review of the possible associations between ambient PM2.5 exposures and the development of Alzheimer's disease. Ecotoxicol Environ Saf. 2019;174:344-52. Epub 2019/03/05. doi: 10.1016/j.ecoenv.2019.02.086. PubMed PMID: 30849654.

20. Xia T, Zhu Y, Mu L, Zhang ZF, Liu S. Pulmonary diseases induced by ambient ultrafine and engineered nanoparticles in twenty-first century. Natl Sci Rev. 2016;3(4):416-29. Epub 2016/10/08. doi: 10.1093/nsr/nww064. PubMed PMID: 28649460; PubMed Central PMCID: PMC5473351.

21. Zhu X, Ji X, Shou Y, Huang Y, Hu Y, Wang H. Recent advances in understanding the mechanisms of PM(2.5)-mediated neurodegenerative diseases. Toxicol Lett. 2020;329:31-7. Epub 2020/04/29. doi: 10.1016/j.toxlet.2020.04.017. PubMed PMID: 32360789.

22. Block ML, Calderón-Garcidueñas L. Air pollution: mechanisms of neuroinflammation and CNS disease. Trends Neurosci. 2009;32(9):506-16. Epub 2009/08/26. doi: 10.1016/j.tins.2009.05.009. PubMed PMID: 19716187; PubMed Central PMCID: PMC2743793.

23. Münzel T, Gori T, Al-Kindi S, Deanfield J, Lelieveld J, Daiber A, et al. Effects of gaseous and solid constituents of air pollution on endothelial function. Eur Heart J. 2018;39(38):3543-50. doi: 10.1093/eurheartj/ehy481. PubMed PMID: 30124840; PubMed Central PMCID: PMC6174028.

24. Babadjouni R, Patel A, Liu Q, Shkirkova K, Lamorie-Foote K, Connor M, et al. Nanoparticulate matter exposure results in neuroinflammatory changes in the corpus callosum. PLoS One. 2018;13(11):e0206934. Epub 2018/11/05. doi: 10.1371/journal.pone.0206934. PubMed PMID: 30395590; PubMed Central PMCID: PMC6218079.

25. Elder A, Gelein R, Silva V, Feikert T, Opanashuk L, Carter J, et al. Translocation of inhaled ultrafine manganese oxide particles to the central nervous system. Environ Health Perspect. 2006;114(8):1172-8. doi: 10.1289/ehp.9030. PubMed PMID: 16882521; PubMed Central PMCID: PMC1552007.

26. Hesterberg TW, Long CM, Lapin CA, Hamade AK, Valberg PA. Diesel exhaust particulate (DEP) and nanoparticle exposures: what do DEP human clinical studies tell us about potential human health hazards of nanoparticles? Inhal Toxicol. 2010;22(8):679-94. doi: 10.3109/08958371003758823. PubMed PMID: 20462394.

27. Liu NM, Miyashita L, Maher BA, McPhail G, Jones CJP, Barratt B, et al. Evidence for the presence of air pollution nanoparticles in placental tissue cells. Sci Total Environ. 2021;751:142235. Epub 2020/09/12. doi: 10.1016/j.scitotenv.2020.142235. PubMed PMID: 33181987.

28. Maher BA, Ahmed IA, Karloukovski V, MacLaren DA, Foulds PG, Allsop D, et al. Magnetite pollution nanoparticles in the human brain. Proc Natl Acad Sci U S A. 2016;113(39):10797-801. Epub 2016/09/06. doi: 10.1073/pnas.1605941113. PubMed PMID: 27601646; PubMed Central PMCID: PMC5047173.

29. Miller MR, Raftis JB, Langrish JP, McLean SG, Samutrtai P, Connell SP, et al. Inhaled Nanoparticles Accumulate at Sites of Vascular Disease. ACS Nano. 2017;11(5):4542-52. Epub 2017/04/26. doi: 10.1021/acsnano.6b08551. PubMed PMID: 28443337; PubMed Central PMCID: PMC5444047.

30. Hopkins LE, Laing EA, Peake JL, Uyeminami D, Mack SM, Li X, et al. Repeated Iron-Soot Exposure and Nose-to-brain Transport of Inhaled Ultrafine Particles. Toxicol Pathol. 2018;46(1):75-84. Epub 2017/09/15. doi: 10.1177/0192623317729222. PubMed PMID: 28914166; PubMed Central PMCID: PMC6405220.

31. Gao M, Cao J, Seto E. A distributed network of low-cost continuous reading sensors to measure spatiotemporal variations of PM2.5 in Xi'an, China. Environ Pollut. 2015;199:56-65. Epub 2015/01/23. doi: 10.1016/j.envpol.2015.01.013. PubMed PMID: 25618367.

32. Holstius DM, Pillarisetti A, Smith KR, Seto E. Field calibrations of a low-cost aerosol sensor at a regulatory monitoring site in California. Atmos Meas Tech. 2014;7:1121–31. doi: https://doi.org/10.5194/amt-7-1121-2014.

33. Vedal S, Han B, Xu J, Szpiro A, Bai Z. Design of an Air Pollution Monitoring Campaign in Beijing for Application to Cohort Health Studies. Int J Environ Res Public Health. 2017;14(12). Epub 2017/12/15. doi: 10.3390/ijerph14121580. PubMed PMID: 29244738; PubMed Central PMCID: PMC5750998.

34. Bai Y, Brugha RE, Jacobs L, Grigg J, Nawrot TS, Nemery B. Carbon loading in airway macrophages as a biomarker for individual exposure to particulate matter air pollution - A critical review. Environ Int. 2015;74:32-41. doi: 10.1016/j.envint.2014.09.010. PubMed PMID: 25318022.

35. Saenen ND, Bové H, Steuwe C, Roeffaers MBJ, Provost EB, Lefebvre W, et al. Children's Urinary Environmental Carbon Load. A Novel Marker Reflecting Residential Ambient Air Pollution Exposure? Am J Respir Crit Care Med. 2017;196(7):873-81. doi: 10.1164/rccm.201704-0797OC. PubMed PMID: 28686472.
36. Romero G, Rojas E, Estrela-Lopis I, Donath E, Moya SE. Spontaneous confocal Raman microscopy--a tool to study the uptake of nanoparticles and carbon nanotubes into cells. Nanoscale Res Lett. 2011;6:429. Epub 2011/06/16. doi: 10.1186/1556-276X-6-429. PubMed PMID: 21711493; PubMed Central PMCID: PMC3211846.
37. Bi Y, Yang C, Chen Y, Yan S, Yang G, Wu Y, et al. Near-resonance enhanced label-free stimulated Raman scattering microscopy with spatial resolution near 130 nm. Light Sci Appl. 2018;7:81. Epub 2018/10/24. doi: 10.1038/s41377-018-0082-1. PubMed PMID: 30374403; PubMed Central PMCID: PMC6199294.
38. Francis AT, Nguyen TT, Lamm MS, Teller R, Forster SP, Xu W, et al. In Situ Stimulated Raman Scattering (SRS) Microscopy Study of the Dissolution of Sustained-Release Implant Formulation. Molecular Pharmaceutics. 2018;15(12):5793-801.
39. Freudiger CW, Min W, Saar BG, Lu S, Holtom GR, He C, et al. Label-free biomedical imaging with high sensitivity by stimulated Raman scattering microscopy. Science. 2008;322(5909):1857-61. doi: 10.1126/science.1165758. PubMed PMID: 19095943; PubMed Central PMCID: PMC3576036.
40. Fu D. Quantitative chemical imaging with stimulated Raman scattering microscopy. Curr Opin Chem Biol. 2017;39:24-31. Epub 2017/05/22. doi: 10.1016/j.cbpa.2017.05.002. PubMed PMID: 28544970.
41. Fung AA, Shi L. Mammalian cell and tissue imaging using Raman and coherent Raman microscopy. Wiley Interdiscip Rev Syst Biol Med. 2020;12(6):e1501. Epub 2020/07/19. doi: 10.1002/wsbm.1501. PubMed PMID: 32686297; PubMed Central PMCID: PMC7554227.
42. Hill AH, Fu D. Cellular Imaging Using Stimulated Raman Scattering Microscopy. Anal Chem. 2019;91(15):9333-42. Epub 2019/07/09. doi: 10.1021/acs.analchem.9b02095. PubMed PMID: 31287649.
43. Laptenok SP, Rajamanickam VP, Genchi L, Monfort T, Lee Y, Patel II, et al. Fingerprint-to-CH stretch continuously tunable high spectral resolution stimulated Raman scattering microscope. J Biophotonics. 2019;12(9):e201900028. Epub 2019/06/14. doi: 10.1002/jbio.201900028. PubMed PMID: 31081280.
44. Lee HJ, Cheng JX. Imaging chemistry inside living cells by stimulated Raman scattering microscopy. Methods. 2017;128:119-28. Epub 2017/07/23. doi: 10.1016/j.ymeth.2017.07.020. PubMed PMID: 28746829.
45. Prince RC, Frontiera RR, Potma EO. Stimulated Raman Scattering: From Bulk to Nano. Chem Rev. 2017;117(7):5070-94. Epub 2016/12/14. doi: 10.1021/acs.chemrev.6b00545. PubMed PMID: 27966347; PubMed Central PMCID: PMC5471143.
46. Wei L, Hu F, Chen Z, Shen Y, Zhang L, Min W. Live-Cell Bioorthogonal Chemical Imaging: Stimulated Raman Scattering Microscopy of Vibrational Probes. Acc Chem Res. 2016;49(8):1494-502. Epub 2016/08/03. doi: 10.1021/acs.accounts.6b00210. PubMed PMID: 27486796; PubMed Central PMCID: PMC5704954.
47. Kukull WA, Higdon R, Bowen JD, McCormick WC, Teri L, Schellenberg GD, et al. Dementia and Alzheimer disease incidence: a prospective cohort study. Arch Neurol. 2002;59:1737-46.
48. Shaffer RM, Li G, Adar SD, Dirk Keene C, Latimer CS, Crane PK, et al. Fine Particulate Matter and Markers of Alzheimer's Disease Neuropathology at Autopsy in a Community-Based Cohort. J Alzheimers Dis.

2021;79(4):1761-73. doi: 10.3233/JAD-201005. PubMed PMID: 33459717; PubMed Central PMCID: PMC8061707.

49. Sampson PD, Richards M, Szpiro AA, Bergen S, Sheppard L, Larson TV, et al. A regionalized national universal kriging model using Partial Least Squares regression for estimating annual PM. Atmos Environ (1994). 2013;75:383-92. doi: 10.1016/j.atmosenv.2013.04.015. PubMed PMID: 24015108; PubMed Central PMCID: PMC3763950.

50. Szpiro AA, Sampson PD, Sheppard L, Lumley T, Adar SD, Kaufman J. Predicting Intra-Urban Variation in Air Pollution Concentrations with Complex Spatio-Temporal Dependencies. Environmetrics. 2009;21(6):606-31. doi: 10.1002/env.1014. PubMed PMID: 24860253; PubMed Central PMCID: PMC4029437.

51. Kukull WA, Higdon R, Bowen JD, McCormick WC, Teri L, Schellenberg GD, et al.

52. Watson AY, Valberg PA. Carbon black and soot: Two different substances. *AIHAJ : A Journal for the Science of Occupational and Environmental Health and Safety*. 2001;62(2):218-28.

53. Canagaratna MR, Massoli P, Browne EC, Franklin JP, Wilson KR, Onasch TB, et al. Chemical compositions of black carbon particle cores and coatings via soot particle aerosol mass spectrometry with photoionization and electron ionization. J Phys Chem A. 2015;119(19):4589-99. Epub 2015/01/15. doi: 10.1021/jp510711u. PubMed PMID: 25526741.

54. Castro LM, Pio CA, Harrison RM, Smith DJT. Carbonaceous aerosol in urban and rural European atmospheres: estimation of secondary organic carbon concentrations. Atmospheric Environment. 1999;33 (17):2771-81.

55. Gould T, Larson T, Stewart J, Kaufman JD, Slater D, McEwen N. A controlled inhalation diesel exhaust exposure facility with dynamic feedback control of PM concentration. Inhal Toxicol. 2008;20(1):49-52. doi: 10.1080/08958370701758478. PubMed PMID: 18236222.

56. Figueroa B, Nguyen T, Sotthivirat S, Xu W, Rhodes T, Lamm MS, et al. Detecting and Quantifying Microscale Chemical Reactions in Pharmaceutical Tablets by Stimulated Raman Scattering Microscopy. Anal Chem. 2019;91(10):6894-901. Epub 2019/04/30. doi: 10.1021/acs.analchem.9b01269. PubMed PMID: 31009215.

57. Figueroa B, Chen Y, Berry K, Francis A, Fu D. Label-Free Chemical Imaging of Latent Fingerprints with Stimulated Raman Scattering Microscopy. Anal Chem. 2017;89(8):4468-73. Epub 2017/03/31. doi: 10.1021/acs.analchem.6b04213. PubMed PMID: 28322553.

58. Preibisch S, Saalfeld S, Tomancak P. Globally optimal stitching of tiled 3D microscopic image acquisitions. Bioinformatics. 2009;25(11):1463-5. Epub 2009/04/03. doi: 10.1093/bioinformatics/btp184. PubMed PMID: 19346324; PubMed Central PMCID: PMC2682522.

59. CA G. An Analysis of Histogram-based Thresholding Algorithms. CVGIP:Graphical Models and image processing. 1993;55:532-7.

60. Krombach F, Münzing S, Allmeling AM, Gerlach JT, Behr J, Dörger M. Cell size of alveolar macrophages: an interspecies comparison. Environ Health Perspect. 1997;105 Suppl 5(Suppl 5):1261-3. Epub 1997/12/24. doi: 10.1289/ehp.97105s51261. PubMed PMID: 9400735; PubMed Central PMCID: PMC1470168.

61. Haley PJ, Muggenburg BA, Weissman DN, Bice DE. Comparative morphology and morphometry of alveolar macrophages from six species. Am J Anat. 1991;191(4):401-7. doi: 10.1002/aja.1001910407. PubMed PMID: 1951138.

62. Bové H, Steuwe C, Fron E, Slenders E, D'Haen J, Fujita Y, et al. Biocompatible Label-Free Detection of Carbon Black Particles by Femtosecond Pulsed Laser Microscopy. Nano Lett. 2016;16(5):3173-8. Epub 2016/04/22. doi: 10.1021/acs.nanolett.6b00502. PubMed PMID: 27104759.

63. Bové H, Bongaerts E, Slenders E, Bijnens EM, Saenen ND, Gyselaers W, et al. Ambient black carbon particles reach the fetal side of human placenta. Nat Commun. 2019;10(1):3866. Epub 2019/09/17. doi: 10.1038/s41467-019-11654-3. PubMed PMID: 31530803; PubMed Central PMCID: PMC6748955.

64. Otsu N. A Threshold Selection Method from Gray-Level Histograms. *IEEE Transactions on Systems, Man, and Cybernetics*. 1979;9(1):62-6. doi: 10.1109/TSMC.1979.4310076.

65. Oberdörster G, Sharp Z, Atudorei V, Elder A, Gelein R, Kreyling W, et al. Translocation of inhaled ultrafine particles to the brain. Inhal Toxicol. 2004;16(6-7):437-45. doi: 10.1080/08958370490439597. PubMed PMID: 15204759.